

Alanine Racemase Free Energy Profiles from Global Analyses of Progress Curves

M. Ashley Spies,[†] Joshua J. Woodward,[†] Mitchell R. Watnik,[‡] and Michael D. Toney^{*,†}

Contribution from the Department of Chemistry and Statistical Laboratory, University of California, One Shields Avenue, Davis, California 95616

Received January 23, 2004; E-mail: mdtoney@ucdavis.edu

Abstract: Free energy profiles for alanine racemase from *Bacillus stearothermophilus* have been determined at pH 6.9 and 8.9 from global analysis of racemization progress curves. This required a careful statistical design due to the problems in finding the global minimum in mean square for a system with eight adjustable parameters (i.e., the eight rate constants that describe the stepwise chemical mechanism). The free energy profiles obtained through these procedures are supported by independent experimental evidence: (1) steady-state kinetic constants, (2) solvent viscosity dependence, (3) spectral analysis of reaction intermediates, (4) equilibrium overshoots for progress curves measured in D₂O, and (5) the magnitudes of calculated intrinsic kinetic isotope effects. The free energy profiles for the enzyme are compared to those of the uncatalyzed and the PLP catalyzed reactions. At pH 6.9, PLP lowers the free energy of activation for deprotonation by 8.4 kcal/mol, while the inclusion of apoenzyme along with PLP additionally lowers it by 11 kcal/mol.

Introduction

D-Alanine is an essential component of bacterial cell walls, which are rigid structures composed of cross-links between polysaccharides and peptides.¹ The bacterial cell wall affords protection from osmotic lysis, and thus its biosynthetic pathways represent attractive targets for antibiotic development.² D-Alanine and D-glutamate are constituents of the peptidoglycan layer and are thought to confer resistance to protease digestion.² The readily available form of alanine in bacteria is the L-stereoisomer, which is racemized to the D-stereoisomer by alanine racemase (E. C. 5.1.1.1). This is the first step in the synthesis of the D-Ala-D-Ala component of peptidoglycan, the second and third steps being the ligation of D-Ala to provide the D-Ala-D-Ala dipeptide and the ATP-dependent addition of the D-Ala-D-Ala dipeptide to L-Lys on the growing peptidoglycan, respectively.¹

Alanine racemase employs pyridoxal phosphate (PLP) as a cofactor. Amino acid substrates react with PLP to form aldimine intermediates, the C α protons of which have greatly reduced pK_a values.³ It has been established that alanine racemase from *Bacillus stearothermophilus* utilizes a two-base mechanism in which Tyr265 and Lys39 act as general acid/base catalysts.^{4–6}

Racemization in the L \rightarrow D direction is accomplished by the Tyr265 catalyzed proton abstraction from C α of the aldimine followed by transfer of a solvent-derived proton from Lys39 to the opposite face, yielding the antipodal aldimine (Scheme 1). In the D \rightarrow L direction, proton abstraction is catalyzed by Lys39, while the solvent-derived proton is donated by Tyr265. Recent multiple hydrogen kinetic isotope effects established that alanine racemase catalyzed racemization occurs through an obligatory carbanionic intermediate rather than bypassing this intermediate in a concerted mechanism (Scheme 1).⁷

The elucidation of the chemical mechanism opens the door to the definition of the free energy profile for alanine racemase. Free energy profiles for enzymatic reactions are generally difficult to define due to the complex, multistep natures of the mechanisms. It has been accomplished for several enzymes, with the work of Knowles et al. on triose phosphate isomerase^{8–14} and proline racemase^{15–20} being excellent examples. These series

[†] Department of Chemistry.

[‡] Statistical Laboratory.

(1) Neidhart, F. C. *Escherichia coli and Salmonella*, 2nd ed.; Blackwell Publishing: London, 1999.

(2) Walsh, C. T. *J. Biol. Chem.* **1989**, *264*, 2393–6.

(3) Dixon, J. E.; Bruice, T. C. *Biochemistry* **1973**, *12*, 4762–6.

(4) Watanabe, A.; Yoshimura, T.; Mikami, B.; Esaki, N. *J. Biochem.* **1999**, *126*, 781–786.

(5) Watanabe, A.; Kurokawa, Y.; Yoshimura, T.; Kurihara, T.; Soda, K.; Esaki, N. *J. Biol. Chem.* **1999**, *274*, 30334.

(6) Sun, S. X.; Toney, M. D. *Biochemistry* **1999**, *38*, 4058–4065.

(7) Spies, M. A.; Toney, M. D. *Biochemistry* **2003**, *42*, 5099–107.

(8) Albery, W. J.; Knowles, J. R. *Biochemistry* **1976**, *15*, 5631–40.

(9) Herlihy, J. M.; Maister, S. G.; Albery, W. J.; Knowles, J. R. *Biochemistry* **1976**, *15*, 5601–7.

(10) Maister, S. G.; Pett, C. P.; Albery, W. J.; Knowles, J. R. *Biochemistry* **1976**, *15*, 5607–12.

(11) Fletcher, S. J.; Herlihy, J. M.; Albery, W. J.; Knowles, J. R. *Biochemistry* **1976**, *15*, 5612–7.

(12) Leadlay, P. F.; Albery, W. J.; Knowles, J. R. *Biochemistry* **1976**, *15*, 5617–20.

(13) Fisher, L. M.; Albery, W. J.; Knowles, J. R. *Biochemistry* **1976**, *15*, 5621–6.

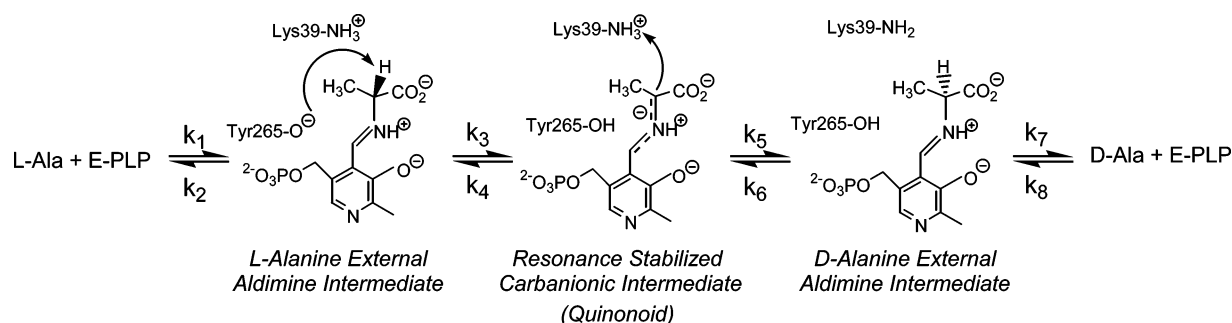
(14) Albery, W. J.; Knowles, J. R. *Biochemistry* **1976**, *15*, 5627–31.

(15) Fisher, L. M.; Albery, W. J.; Knowles, J. R. *Biochemistry* **1986**, *25*, 2529–37.

(16) Belasco, J. G.; Bruice, T. W.; Fisher, L. M.; Albery, W. J.; Knowles, J. R. *Biochemistry* **1986**, *25*, 2564–71.

(17) Belasco, J. G.; Bruice, T. W.; Albery, W. J.; Knowles, J. R. *Biochemistry* **1986**, *25*, 2558–64.

Scheme 1



of classic papers employed experiments based on complex analytical mathematics to obtain the free energy profiles. In other cases, detailed pre-steady-state experiments commonly form the core analysis. Examples include tyrosyl-tRNA synthetase,²¹ dihydrofolate reductase,^{22–24} S-adenosylmethionine synthetase,²⁵ 3-oxo- Δ^5 -steroid isomerase,²⁶ pyruvate phosphate dikinase,²⁷ aspartate aminotransferase,²⁸ horse liver alcohol dehydrogenase,²⁹ and dialkylglycine decarboxylase.³⁰ It would be advantageous to have a generalized and straightforward framework for determining enzymatic free energy profiles from data that are relatively simple to collect, rather than treating mathematically each enzyme mechanism individually to determine appropriate experiments or designing and performing comprehensive pre-steady-state kinetic analyses. This is accomplished here for alanine racemase by taking advantage of recently available, robust global data analysis methods and the reversibility of the racemization reaction. It is shown herein that a series of complete racemization progress curves contains full free energy profile information, which can be extracted by straightforward statistical procedures relying on global data analysis. It is expected that this methodology will be applicable to reversible enzyme catalyzed reactions in general, making determination of free energy profiles from progress curves a common task.

Experimental Section

Materials. D- and L-alanine were purchased from Aldrich (99% pure). Buffers and sucrose were from Fisher. Alanine racemase from *Bacillus stearothermophilus* was prepared as previously described.⁶ Deuterium oxide (99.9 atom %) was purchased from Cambridge Isotope Laboratories Inc.

Progress Curves. A Jasco 720 circular dichroism spectrophotometer was used for all studies. The wavelength used (215 nm) was chosen

such that the CD signal was linear with amino acid concentration. Data acquisition employed the Jasco program J-700 under the Windows Hardware Manager, version 1.10.00. Initial D- and L-alanine concentrations were varied from 0.2 to 20 mM ($0.1–10 \times K_M$). The buffer was either 50 mM potassium phosphate (pH 6.9) or 50 mM potassium borate (pH 8.9), with 100 mM potassium chloride. The temperature was 25 °C. Enzyme concentration was varied from 5 to 26 nM for the pH 8.9 data and from 10 to 100 nM for the pH 6.9 data.

Viscosity Variation Studies. The k_{cat}/K_M values for the D→L direction were determined by initial rate methods as a function of solvent viscosity using sucrose as viscogen. A coupled enzyme assay was employed for the pH 8.9 and 10.5 data, as previously described.⁶ The CD assay was employed for the pH 6.9 data. Relative viscosities were calculated from literature aqueous sucrose viscosity data.^{31,32} The buffer was 50 mM potassium phosphate (pH 6.9), 100 mM CHES (pH 8.9), or 100 mM CAPS (pH 10.5). All solutions contained 100 mM potassium chloride. The temperature was 25 °C.

Racemization Progress Curves for Protiated D- and L-Alanine in D₂O. The D₂O progress curves were measured by CD, as described for the H₂O progress curves. The buffer was 50 mM potassium borate, 100 mM potassium chloride, pD 8.9, and the temperature was 25 °C. The alanine racemase concentration was 44 nM. Enzyme was added to either 11 mM protiated L-alanine or 17 mM protiated D-alanine to start the reaction.

Data Analysis. DynaFit 3.25.00 was used for global fitting of progress curves.³³ Randomized sets of rate constants and calculated steady-state kinetic constants were generated with Kaleidagraph 3.5. Derivation of steady-state velocity equations was performed by the net rate constant method of Cleland.³⁴

Computational Procedures

(A) General Approach. Computer programs such as KINSIM/FITSIM and DynaFit are powerful data analysis tools. These programs allow the simulation of progress curves for complex chemical mechanisms. The user simply enters a mechanism in graphical format, and these programs extract the differential equations that describe the system and integrate them for the specified initial starting conditions and time frame. Additionally, they iteratively compare the simulated to the observed timecourse and adjust the values of the rate constants to achieve an optimal fit between the two (i.e., they perform nonlinear regression). They are most frequently employed for the analysis of pre-steady-state (e.g., stopped-flow and quenched-flow) data, although they are equally capable of simulating longer time scales such as those typically found in enzymatic progress curve measurements. DynaFit is a particularly robust program that allows the user to fit simultaneously

- (18) Belasco, J. G.; Albery, W. J.; Knowles, J. R. *Biochemistry* **1986**, *25*, 2552–8.
- (19) Fisher, L. M.; Belasco, J. G.; Bruice, T. W.; Albery, W. J.; Knowles, J. R. *Biochemistry* **1986**, *25*, 2543–51.
- (20) Fisher, L. M.; Albery, W. J.; Knowles, J. R. *Biochemistry* **1986**, *25*, 2538–42.
- (21) Wells, T. N.; Ho, C. K.; Fersht, A. R. *Biochemistry* **1986**, *25*, 6603–8.
- (22) Fierke, C. A.; Johnson, K. A.; Benkovic, S. J. *Biochemistry* **1987**, *26*, 4085–92.
- (23) Rajagopalan, P. T.; Lutz, S.; Benkovic, S. J. *Biochemistry* **2002**, *41*, 12618–28.
- (24) Benkovic, S. J.; Fierke, C. A.; Naylor, A. M. *Science* **1988**, *239*, 1105–10.
- (25) McQueney, M. S.; Anderson, K. S.; Markham, G. D. *Biochemistry* **2000**, *39*, 4443–54.
- (26) Hawkinson, D. C.; Eames, T. C.; Pollack, R. M. *Biochemistry* **1991**, *30*, 10849–58.
- (27) Mehl, A.; Xu, Y.; Dunaway-Mariano, D. *Biochemistry* **1994**, *33*, 1093–102.
- (28) Goldberg, J. M.; Kirsch, J. F. *Biochemistry* **1996**, *35*, 5280–91.
- (29) Adolph, H. W.; Maurer, P.; Schneider-Bernlohr, H.; Sartorius, C.; Zeppezauer, M. *Eur. J. Biochem.* **1991**, *201*, 615–25.
- (30) Zhou, X.; Jin, X.; Medhekar, R.; Chen, X.; Dieckmann, T.; Toney, M. D. *Biochemistry* **2001**, *40*, 1367–77.

- (31) Lide, D. R. *CRC Handbook of chemistry and physics: a ready-reference book of chemical and physical data*, 73rd ed.; CRC Press: Boca Raton, FL, 1992.
- (32) Bazelyansky, M.; Robey, E.; Kirsch, J. F. *Biochemistry* **1986**, *25*, 125–30.
- (33) Kuzmic, P. *Anal. Biochem.* **1996**, *237*, 260–73.
- (34) Cleland, W. W. *Biochemistry* **1975**, *14*, 3220–4.

multiple data sets each with independent starting conditions (e.g., substrate concentration). DynaFit was chosen for the present application due to its flexibility, ease of use, robustness, statistical features, and scripting abilities.

Enzyme kineticists have traditionally shunned progress curve analyses due to the difficulties in integrating the equations for complex mechanisms and applying the resulting complicated integrated rate equations to data analysis. This is not to say that integrated rate equations have not been successfully employed in enzymology.³⁵ With the advent of programs such as DynaFit, these integration and data analysis difficulties for progress curves are eliminated. One can collect a large number of full progress curves that differ in, for example, initial substrate concentration. These can be read into DynaFit and fitted to the chemical mechanism describing the enzyme under analysis, yielding best-fit estimates for the microscopic rate constants of the mechanism through a straightforward procedure.

Alanine racemase is particularly amenable to this treatment, due to the kinetic simplicity (one substrate and one product) and the definite equilibrium constant of unity. Additionally, the chemical mechanism of the enzyme was recently shown to be a stepwise double proton transfer by multiple kinetic isotope effects (KIEs).⁷ The fits obtained from global analyses of multiple progress curves can be confirmed by a variety of independent measurements with alanine racemase. For example, steady-state kinetic constants (e.g., k_{cat} , K_M) are known aggregates of the microscopic rate constants (the fitted parameters in the present procedure) describing the mechanism. Values for these steady-state constants are easily obtained from initial rate experiments and can be compared to those calculated from the fitted rate constants. The effect of viscosity variation, which generally probes the contributions of bimolecular steps to rate limitation, offers additional validation. Other independent measurements that can be used as checks on the fitted rate constants include spectroscopic analysis of enzyme intermediates under substrate-saturating equilibrium conditions, KIEs, and the presence or absence of "overshoots" in progress curves conducted in D_2O .

The application of nonlinear regression to kinetic analyses is straightforward when relatively simple, well-behaved equations and data with a strong signal are employed. The difficulty increases greatly as the number of fitted rate constants increases.³⁶ Thus, in fitting data to a mechanism with, for example, eight rate constants, it is a challenge to find the set of values that gives the global minimum on the mean square hypersurface. Here, this problem of finding the global minimum is addressed by starting the search for the optimal set of rate constants with the screening of quasi-randomly generated sets of rate constants. Sets that yield values of steady-state kinetic constants not too distant from experimentally determined values are selected for full global analysis. The rate constants of the selected sets are used as initial estimates in global fits to a group of experimental progress curves. Those globally fitted sets of rate constants that are in close accord with experimental data (e.g. equilibrium constant) are selected and averaged together, and this averaged set of rate constants is used as initial estimates in a further global fit.

The hypersurface about the apparent minimum is explored to ensure that the global minimum has been reached by randomizing the fitted rate constants by a small fraction and then globally refitting these randomized rate constant sets. If the true minimum has been reached, then these will reconverge on the original solution. This set of optimized rate constants is used to construct the free energy profile for the enzyme, which is itself validated by independent experimental data.

(B) Specific Methodology. Screening of Quasi-Randomized Sets of Rate Constants. The screening procedure employed 1000 quasi-randomly generated sets of rate constants. The stepwise mechanism is defined by eight rate constants (Scheme 1). The limits on the

randomization were as follows: k_1 and k_8 , 5×10^4 – $5 \times 10^7 \text{ M}^{-1} \text{ s}^{-1}$; k_2 , k_3 , k_6 , and k_7 , 50 – $50\,000 \text{ s}^{-1}$; k_4 and k_5 , 1×10^7 – $1 \times 10^{10} \text{ s}^{-1}$. Rate constant sets for which any one of the four calculated steady-state parameters (two k_{cat} and two K_M values) fell outside of the range of 50–150% of the experimental values were eliminated from further consideration. For the pH 8.9 and 6.9 sets, this resulted in 160 and 214 parameter sets, respectively, being selected for initial global fitting.

Batch Global Fitting of Screened Rate Constant Sets. The selected rate constant sets were fitted in batch mode using DynaFit. This requires only an input script from the user, enabling a large number of fits to be executed automatically. No constraints were placed on the rate constants during the fitting procedure, and all eight rate constants were fitted. A modification of the default settings for DynaFit was used. A stopping criterion for the Marquardt compromise parameter (λ) was employed ($\text{StopLambda} = 1 \times 10^{-7}$), and the Levenberg–Marquardt algorithm was set to restart once an apparent minimum had been reached ($\text{Restarts} = 5$). Also, DynaFit can adjust the initial concentrations of the reacting species (alanine and enzyme) up to 10% from the input values to correct for pipetting errors. This feature was used in this initial phase of the fitting process.

Steady-state kinetic parameters were calculated from the fitted microscopic rate constants and were compared to the experimental values. Fitted rate constant sets were selected based on both the calculated steady-state parameters (k_{cat} 's, K_M 's, and the equilibrium constant) and the mean square value. The mean square is defined as the sum over all data points of the square of the difference between the predicted and observed value divided by the total number of data points. DynaFit provides the option of weighting individual progress curves within the global data set. The default setting ($\text{Equalize} = 1$) was used, which ensures that each progress curve contributes equally to the global fit even though the curves do not contain identical numbers of data points. For the pH 8.9 data set, rate constant sets were eliminated if the values of any of the calculated steady-state kinetic parameters fell outside of the range of 50–150% of the experimental values or had mean square values larger than 1.02. This yielded three parameter sets. All of these selected sets had calculated equilibrium constants within 20% of unity. These three sets were then averaged, resulting in the "averaged" rate constant set for pH 8.9 (Table 2). For pH 6.9, rate constant sets were eliminated if the values of any of the calculated steady-state kinetic parameters fell outside of the range of 50% to 150% of the experimental and had mean square values larger than 1.7.

Refinement of Averaged Rate Constant Set. The averaged set is likely to be near the values that give the global minimum of mean square. Thus, the averaged rate constant set is used as initial rate constants in an additional fit, yielding the "averaged-fitted" rate constant set (Table 2). To examine more systematically the hypersurface around the averaged-fitted rate constant set, the rate constants were each randomized by 5%, to generate 70 new rate constant sets, which were then independently globally fitted. It was found that the 10% titration in initial substrate and enzyme concentrations had a deleterious effect on the ability of the algorithm to optimize the 5% randomized rate constant sets to closely similar fits, yielding mean square values that spanned a large range. Convergence is greatly improved when the titration feature is turned off. Furthermore, the value of any given rate constant varies only slightly between fitted rate constant sets when the 5% randomized sets are used as initial estimates. The same procedure was employed for the pH 6.9 data set, yielding similar results (Table 3). The mean square values spanned a large range when the titration feature is turned on and is greatly reduced when turned off. The "optimized" rate constant sets for the pH 6.9 and 8.9 data are those that gave the lowest mean square values in the fits of the 5% randomized rate constant sets using the tight convergence criteria.

Energy Boundary of the Quinonoid Intermediate. The fitted values for k_4 and k_5 are likely to be the least well determined, since they are most removed from the bimolecular steps that are directly probed by the substrate concentration dependence. Further analysis of

(35) Duggleby, R. G. *Methods Enzymol.* **1995**, *249*, 61–90.

(36) Motulsky, H. J.; Ransnas, L. A. *FASEB J.* **1987**, *1*, 365–74.

Table 1. Experimental and Calculated Steady-State Kinetic Constants^a

	K_M (mM)		$k_{cat} \times 10^{-3}$ (s ⁻¹)		K_{eq}
	L→D	D→L	L→D	D→L	
weighted averages of experimental values ^b	pH 8.9				
	3.3	2.3	1.3	1.0	0.9
calculated values from global fits ^c	(1.0)	(0.4)	(0.5)	(0.2)	(0.5)
	4.5	2.8	1.9	1.0	1.2
experimental values	pH 6.9				
	2.1	1.6	0.21	0.18	0.9
calculated values from global fits ^c	(0.3)	(0.1)	(0.01)	(0.01)	(0.2)
	1.9	1.5	0.23	0.16	1.2
	pH 10.5				
	(0.7)	(0.5)	(0.04)	(0.04)	(0.3)

^a Errors are given in parentheses. Those for the weighted averages of experimental values at pH 8.9 are standard deviations of the individual values that were averaged. Those for the experimental values at pH 6.9 are standard error estimates from nonlinear regression analysis of the initial rate data. Those for the calculated values are propagations of standard errors estimated in the global fits by DynaFit. ^b Weighted average from two published sets of values and one set determined from the initial rates of progress curves. ^c Steady-state values were calculated from the optimized microscopic rate constants using the appropriate expressions for the stepwise mechanism (Scheme 1).

the sensitivity of the fitting procedure to the values of k_4 and k_5 was therefore undertaken. The other six rate constants were held fixed at their values from the optimized rate constant set, while initial values of k_4 and k_5 were varied systematically such that the energy of the quinonoid intermediate ranged from 1.5 to 12.5 kcal/mol. Optimization of k_4 and k_5 required the initial value of the Marquardt compromise parameter λ to be lowered (InitLambda = 0.001), so that the Levenberg–Marquardt algorithm behaves more as the quadratic Gauss–Newton method and less as the steepest descent method. Using the DynaFit default settings, which gives a largely steepest descent character, the Levenberg–Marquardt algorithm was unable to adjust the values of k_4 and k_5 (and thereby the energy of the quinonoid intermediate).

Results

Experimentally Determined Steady-State Kinetic Parameters. The CD progress curves, which were used for global fitting, were also used to obtain initial rates and thereby steady-state rate constants (k_{cat} 's and K_M 's). Two additional sets of steady-state kinetic parameters at pH 8.9 are in the literature.^{6,37} All three were combined in a weighted average to give the values presented in Table 1. These values were used to guide the screening and selection process presented in the Computational Procedures section. For the pH 6.9 data set, the only complete set of experimental steady-state kinetic parameter values are from the initial rates of the progress curves.

Viscosity Variation. A plot of relative viscosity vs relative k_{cat}/K_M values at pH 6.9, 8.9, and 10.5 is shown in Figure 1. These studies show that under alkaline conditions (pH 8.9 and 10.5), there is no significant viscosity effect (pH 8.9 slope = 0.013 ± 0.022), while there is a significant viscosity effect under neutral conditions (pH 6.9 slope = 0.54 ± 0.12). This information provides a valuable check on the accuracy of the free energy profiles constructed from the global fits.

Quinonoid Intermediate Analysis. One can estimate the lower limit on the relative free energy of the quinonoid vs

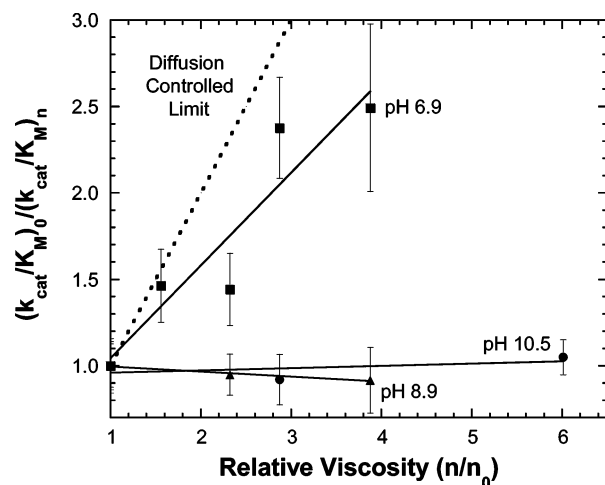


Figure 1. Relative k_{cat}/K_M vs relative viscosity for the D→L direction. The k_{cat}/K_M values were obtained by initial rate methods (see Experimental Section). Sucrose was employed as viscosogen. The dashed line represents the completely diffusion-controlled limit, which has a slope of unity. (●) pH 10.5; (▲) pH 8.9; and (■) pH 6.9. The slope for the pH 6.9 data set is 0.54 ± 0.12 .

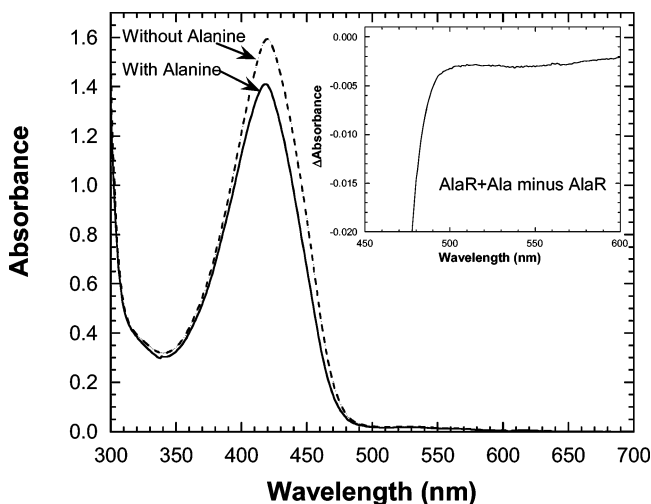


Figure 2. Absorbance spectrum for 280 μ M alanine racemase in the absence and presence of 60 mM (saturating) D,L-alanine, 100 mM potassium borate, pH 8.9, 100 mM KCl. The inset shows the AlaR + Ala minus AlaR difference spectrum in the 450–600 nm region. There is no indication of a positive peak in the 480–530 nm region, which would be indicative of a quinonoid intermediate.

external aldimine intermediates in alanine-saturated alanine racemase knowing the concentration of enzyme, the extinction coefficient, and the spectroscopic limit of detection at the wavelength of interest. Figure 2 shows the spectrum of 280 μ M D,L-alanine-saturated alanine racemase at pH 8.9. The extinction coefficient of the quinonoid intermediate in both enzymatic and nonenzymatic systems is generally approximately $40\,000\text{ M}^{-1}\text{ cm}^{-1}$ ³⁸. The limit of detection in this experiment was estimated to be 0.005 absorbance units at 500 nm (i.e., any deviation of 0.005 absorbance units above the baseline would be easily detectable). No quinonoid intermediate was detected under the present conditions (Figure 2). Thus, the lower limit on the energy of the quinonoid intermediate was calculated to be 4.2 kcal/mol higher than that of the external aldimine intermediates.

Racemization Progress Curves for Protiated D- and L-Alanine in D₂O. The racemization of protiated L- and D-alanine was followed in D₂O at pH 8.9 via circular dichroism.

(37) Faraci, W. S.; Walsh, C. T. *Biochemistry* **1988**, *27*, 3267–76.

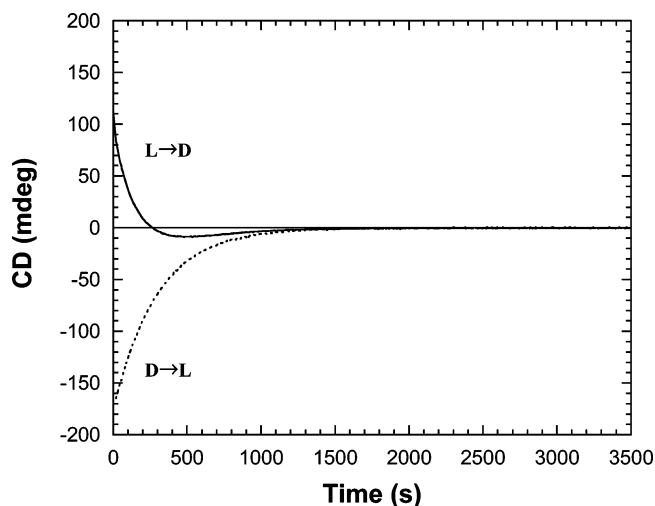


Figure 3. Racemization progress curves for protiated D- and L-alanine in D₂O. The progress curve for the L isomer but not the D isomer shows an “overshoot” of the stereoisomeric equilibrium (i.e., CD = 0).

An “overshoot” of the initial stereoisomeric equilibrium was observed in the L→D direction but not the D→L direction (Figure 3).

Global Analysis of Progress Curves, pH 8.9 Data Set. The procedure described in the Specific Methodology section resulted in three rate constant sets after the initial global fitting to the pH 8.9 data set. These three rate constant sets were averaged, yielding the averaged set presented in Table 2. The estimated standard errors on the rate constants of this averaged set range from approximately 2–25%. Rate constant values from this averaged set were subsequently used as initial estimates in a new global fit, resulting in the averaged-fitted set, also given in Table 2. The rate constants in the averaged-fitted set were each randomized by 5%, generating 70 new sets of initial estimates. These were fitted with the titrations option off. The fitted set with the lowest mean square value (0.5327) was selected as the optimized set. The global fit of the optimized rate constant set to the pH 8.9 data is shown in Figure 4A. A histogram of the mean square values of the randomized and refitted data sets is shown in Figure 5A (mean square = 0.5328 ± 0.0002 , range of values = 0.0006). The inset presents the histogram of the fitted sets with the titration option turned on (mean square = 0.5682 ± 0.0129 ; range of values = 0.08). There is a large reduction in the distribution of mean square and in the average value of mean square when the titration option is turned off. The calculated steady-state rate constants from the optimized rate constant set are presented in Table 1.

Global Analysis of Progress Curves, pH 6.9 Data Set. The same screening and fitting procedure described for the pH 8.9 data set was performed for the pH 6.9 data set. Table 3 presents the averaged and averaged-fitted rate constant sets for pH 6.9. A series of rate constant sets was generated by 5% randomization of the Averaged-Fitted set, as performed with the pH 8.9 set. Figure 5B presents a histogram of mean square values from these fitted sets with the titration option turned off (mean square = 1.314 ± 0.002 , range of values = 0.009), while the inset presents the histogram with the titration option on (mean square = 1.654 ± 0.098 , range of values = 0.4). The rate constant set with the lowest mean square value (1.312) was selected as the optimized set (Table 3). Figure 4B shows the global fits of the

optimized rate constant set to the pH 6.9 data set. The calculated steady-state values from the optimized set are presented in Table 1.

Energy of the Quinonoid Intermediate. To determine the sensitivity of the global fitting procedure to the values of k_4 and k_5 (i.e. quinonoid energy), the other rate constants of the optimized set were held constant, and a series of fits with a range of initial estimates for k_4 and k_5 (constrained by the quinonoid energy) were performed. Figure 6A compares the fitted quinonoid intermediate energies with the initial (input) energies for the pH 8.9 analysis. The results show that, at high quinonoid energies, the global fit under very strict convergence criteria is insensitive to and does not adjust the value of the quinonoid energy. The global fit becomes sensitive to and adjusts the value of the quinonoid energy as the initial energy estimate is decreased. The algorithm increases the fitted value of the quinonoid energy from the initial estimate when the latter is below approximately 4 kcal/mol. Indeed, fitted values form a plateau at approximately 3.2 kcal/mol with lower initial estimates of quinonoid energy. Figure 7A shows the mean square values resulting from the pH 8.9 fits as a function of the fitted quinonoid energies. A flat region exists above approximately 4.5 kcal/mol, while a rise in mean square values occurs below this. The same treatment was employed for the pH 6.9 data set, yielding a fitted vs initial quinonoid energy curve with a lower boundary of 2.5–2.9 kcal/mol (Figure 6B) and a mean square vs fitted quinonoid energy curve showing a flat region above 5 kcal/mol (Figure 7B).

One expects that a perfect algorithm would give, in Figure 6, a perfectly flat region of fitted quinonoid energy below initial quinonoid energy estimates at which the quinonoid intermediate contributes to rate limitation, yet this is not observed. The corollary to this expectation is that, in Figure 7, the mean square values would not have increased above the high energy plateau region, since a perfect algorithm would have raised the fitted quinonoid energies, thereby reducing the mean square. The observed computational results point to imperfections in the implementation of the Levenberg–Marquardt algorithm in DynaFit, since increasing the stringency of the convergence criteria does not affect the computational results.

Free Energy Profiles. The free energy profile for alanine racemase catalysis at pH 8.9, constructed from the optimized rate constant set in Table 2, is shown in Figure 8A. The free energy profile for pH 6.9, constructed from the optimized rate constant set in Table 3, is shown in Figure 9A. Figures 8B and 9B compare the free energy profiles for the enzyme catalyzed reaction with those for the PLP catalyzed and uncatalyzed reactions. The data for the PLP catalyzed and uncatalyzed reactions were taken from the literature.^{3,39,40} There is no available experimental information on the energies of the carbanionic intermediate for the uncatalyzed or PLP catalyzed reactions (or on their existence). Therefore, this intermediate was excluded from the free energy profiles. The $\Delta\Delta G$'s for the pH 8.9 free energy profiles are as follows: 8.6 kcal/mol for uncatalyzed vs PLP catalyzed and 8.7 kcal/mol for PLP

(38) Christen, P.; Metzler, D. E. *Transaminases*; Wiley: New York, 1985; Vol. xxiv, p 643.

(39) French, T. C.; Bruce, T. C. *Biochem. Biophys. Res. Commun.* **1964**, *15*, 403–8.

(40) Rios, A.; Crujeiras, J.; Amyes, T. L.; Richard, J. P. *J. Am. Chem. Soc.* **2001**, *123*, 7949–50.

Table 2. Values of Rate Constants from pH 8.9 Global Fits^a

	$k_1 \times 10^{-6}$ ($M^{-1} s^{-1}$)	$k_2 \times 10^{-3}$ (s^{-1})	$k_3 \times 10^{-3}$ (s^{-1})	$k_4 \times 10^{-8}$ (s^{-1})	$k_5 \times 10^{-8}$ (s^{-1})	$k_6 \times 10^{-3}$ (s^{-1})	$k_7 \times 10^{-3}$ (s^{-1})	$k_8 \times 10^{-6}$ ($M^{-1} s^{-1}$)
averaged ^b	8.92 (2.29)	39.7 (7.5)	2.65 (0.16)	6.64 (2.06)	24.4 (8.1)	4.96 (0.10)	9.61 (1.27)	4.18 (1.03)
averaged-fitted	8.86 (0.44)	39.9 (2.3)	2.63 (0.07)	6.63 (0.47)	24.5 (1.4)	4.94 (0.37)	9.58 (0.69)	4.12 (0.27)
optimized ^c	8.57 (0.39)	44.1 (2.3)	2.68 (0.07)	6.69 (0.54)	22.9 (1.1)	4.76 (0.33)	10.55 (0.56)	3.99 (0.19)

^a Standard error estimates from DynaFit global analyses are given in parentheses. ^b Rate constants are averaged from three different global fits, which converged on a similar solution upon fitting. ^c Final rate constants obtained from nonlinear regression using quasi-randomized rate constants (derived from the averaged-fitted rate constant set) as initial estimates in further global fits.

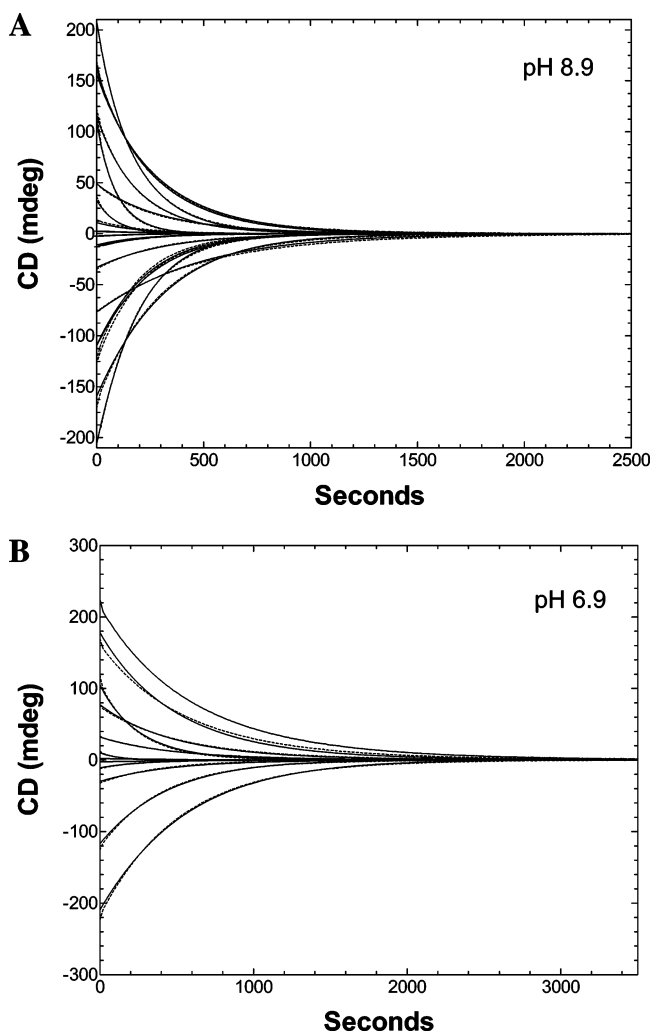


Figure 4. (A) Global fit to pH 8.9 data. Dashed lines, experimental data; solid lines, fitted curves. Positive and negative CD signals correspond to L- and D-alanine, respectively. Fitted rate constant values (optimized) are given in Table 2. (B) Global fit to pH 6.9 data. Fitted rate constant values (optimized) are given in Table 3.

catalyzed vs alanine racemase catalyzed. Those for the pH 6.9 free energy profiles are as follows: 8.4 kcal/mol for uncatalyzed vs PLP catalyzed and 11 kcal/mol for PLP catalyzed vs alanine racemase catalyzed.

Calculation of Intrinsic Kinetic Isotope Effects. One may directly calculate the intrinsic KIE values for alanine racemase using the optimized rate constant set in Table 2 to calculate commitment factors⁴¹ and hydrogen kinetic isotope effects from

previous studies.⁷ Calculated forward commitment factors and the calculated intrinsic substrate KIEs for racemization in both directions at pH 8.9 and 6.9 are presented in Table 4. The reverse commitment, c_r , is zero, since the abstracted proton is irreversibly washed out to solvent.⁴¹ The reverse commitment determines the extent to which the equilibrium isotope effect is expressed in the value of the KIE. Thus, here c_r is effectively zero since there is no equilibrium isotope effect to consider due to isotopic washout. The same calculation may be performed with the solvent isotope effects taken from previous work.⁷ The substrate-derived KIEs for one direction and the solvent-derived KIEs for the opposite direction report on the same proton-transfer transition state. Thus, the substrate-derived D \rightarrow L and solvent-derived L \rightarrow D and the substrate-derived L \rightarrow D and solvent-derived D \rightarrow L report on the same transition states. This is clear from the calculated intrinsic KIE values in Table 4 where the corresponding KIEs are identical within error. Considerations of the equilibrium isotope effects in this analysis are made below.

Discussion

Use of Nonlinear Regression to Obtain Enzymatic Free Energy Profiles. A progress curve, in which the enzyme catalyzed reaction is followed to completion, contains more information than an initial rate measurement, since substrate and product concentrations vary over the course of the measurement. The application of nonlinear regression to progress curve analysis has been successfully employed in a variety of systems over the years to provide estimates of steady-state kinetic constants. These applications have employed either graphical analysis of transformed data based on integrated rate equations⁴² or numerical integration of integrated rate equations for analysis of untransformed data.⁴³ This type of progress curve analysis is generally based on rate equations derived in terms of steady-state constants (e.g., k_{cat} , K_M , and K_I). Thus, the fitted parameters in the nonlinear regression are aggregates of the microscopic rate constants that describe the detailed mechanism.

The approach taken here differs from the historical application of nonlinear regression to progress curve analysis in that the fitted parameters are the microscopic rate constants themselves. Here, DynaFit was employed in the global analysis not of rapid reaction kinetic data but of racemization progress curves in which alanine racemase undergoes many catalytic turnovers. The larger number of fitted parameters (i.e., microscopic rate

(41) O'Leary, M. H. *Annu. Rev. Biochem.* **1989**, *58*, 377–401.

(42) Segel, I. H. *Enzyme kinetics: behavior and analysis of rapid equilibrium and steady-state enzyme systems*; Wiley: New York, 1975; Vol. xxii, p 957.

(43) Straathof, A. J. J. *J. Mol. Catal. B: Enzym.* **2001**, *11*, 991–998.

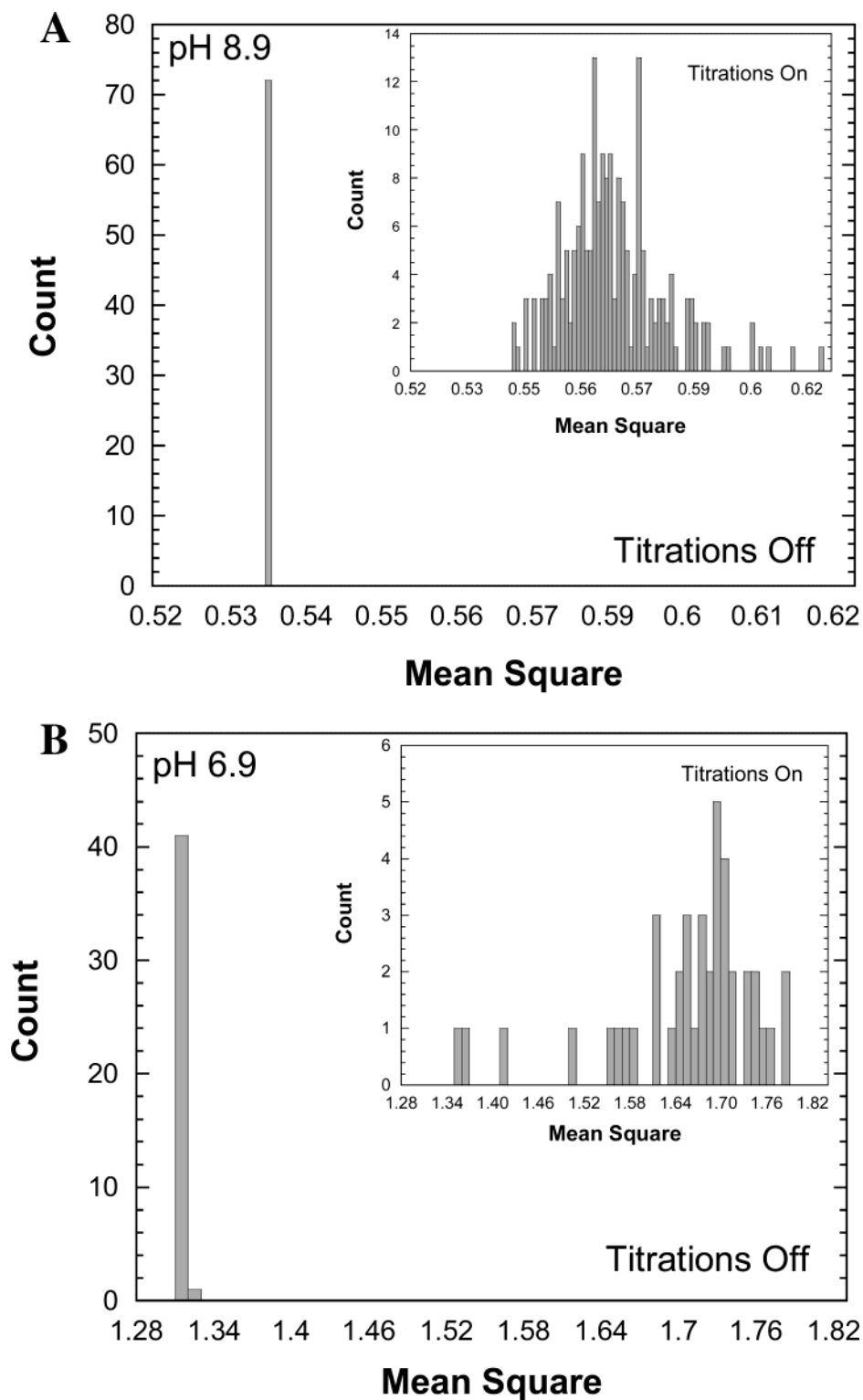


Figure 5. (A) Histogram of mean square values of fitted rate constant sets obtained from randomization about the pH 8.9 averaged-fitted rate constant set (Table 2). The inset shows the mean square histogram generated when the same randomized set is refitted with the titration option turned on. (B) Histogram of mean square values of fitted rate constant sets obtained from randomization about the pH 8.9 averaged-fitted rate constant set (Table 3). The inset shows the mean square histogram generated when the same randomized set is refitted with the titration option turned on.

constants) required appropriate statistical design to ensure that the global minimum in mean square was found. Remarkably, alanine racemase progress curves do indeed contain sufficient information to define the microscopic rate constants in the mechanism, and numerical integration/nonlinear regression can be used to provide accurate values for them.

The statistical procedure used to define the microscopic rate constants consists of five major steps: (1) generation of 1000 rate constant sets in which all rate constant values are randomized within chemically reasonable limits, (2) screening of these quasi-randomized rate constant sets based on steady-state kinetic parameters calculated from them, (3) global fitting of those sets

Table 3. Values of Rate Constants from pH 6.9 Global Fits^a

	$k_1 \times 10^{-5}$ ($M^{-1} s^{-1}$)	$k_2 \times 10^{-2}$ (s^{-1})	$k_3 \times 10^{-2}$ (s^{-1})	$k_4 \times 10^{-8}$ (s^{-1})	$k_5 \times 10^{-8}$ (s^{-1})	$k_6 \times 10^{-2}$ (s^{-1})	$k_7 \times 10^{-2}$ (s^{-1})	$k_8 \times 10^{-5}$ ($M^{-1} s^{-1}$)
averaged ^b	3.22 (0.39)	13.3 (2.5)	13.9 (1.5)	10.0 (1.9)	33.9 (4.1)	13.12 (0.14)	3.90 (0.37)	3.26 (0.44)
averaged-fitted	3.41 (0.26)	12.9 (1.7)	13.3 (1.1)	10.3 (0.1)	32.7 (2.2)	13.45 (0.14)	3.59 (0.12)	3.00 (0.35)
optimized ^c	3.61 (0.21)	12.3 (1.1)	13.2 (2.4)	9.7 (0.1)	30.8 (4.2)	13.90 (0.17)	3.41 (0.23)	3.05 (0.13)

^a Standard error estimates from DynaFit global analyses are given in parentheses. ^b Rate constants are averaged from three different global fits, which converged on a similar solution upon fitting. ^c Final rate constants obtained from nonlinear regression using quasi-randomized rate constants (derived from the averaged-fitted rate constant set) as initial estimates in further global fits.

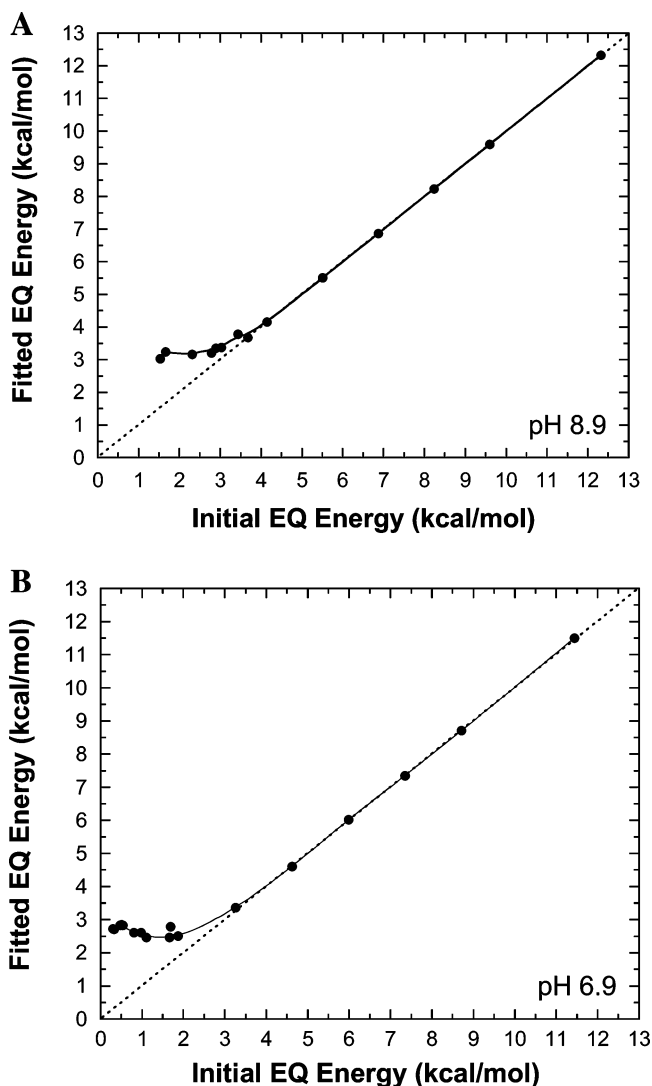


Figure 6. Fitted energy of the quinonoid intermediate as a function of the initial energy input into DynaFit. The values of k_4 and k_5 were fitted, while all others were held at their optimized values. (A) pH 8.9, (B) pH 6.9.

that pass the initial screen, (4) averaging and refitting of convergent solutions, and (5) randomization and refitting to ensure that the global minimum in mean square has been found. The first step randomly distributes sets of rate constant initial estimates across the hypersurface, while the second removes from consideration those sets that are wholly incompatible with the kinetic properties of alanine racemase. The third step constitutes the central discrimination step, while the fourth prevents bias on the part of the experimentalist in choosing among convergent solutions. The fifth step is critical for ensuring

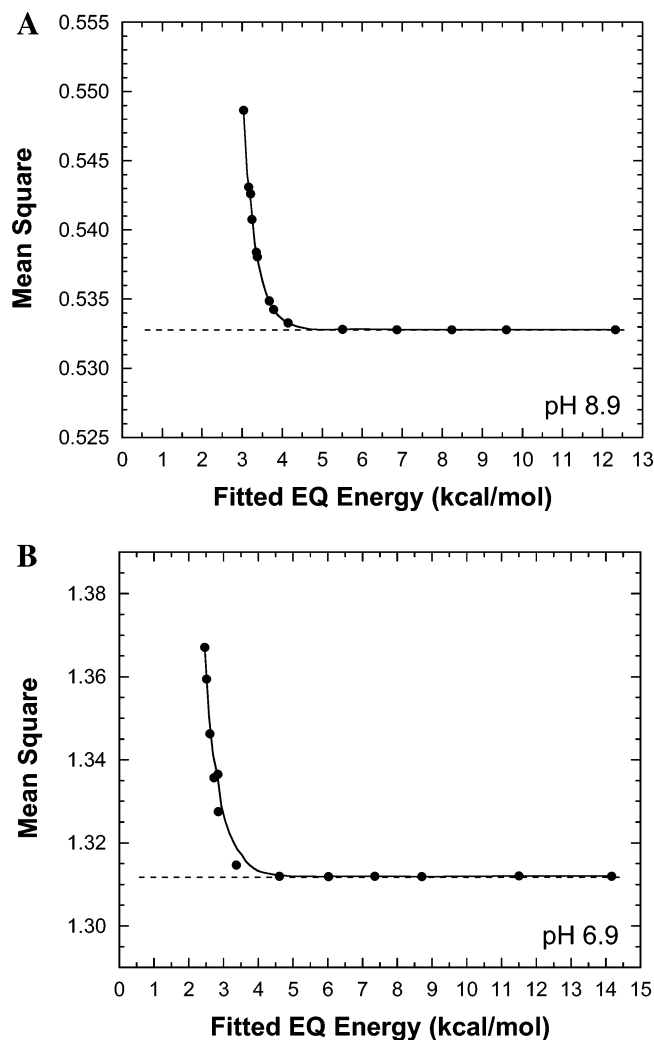


Figure 7. Mean square values as a function of the fitted quinonoid energies. (A) pH 8.9, (B) pH 6.9. The small increase in mean square at the lower values of fitted quinonoid energy is due to the shortcomings of the Levenberg–Marquardt algorithm as implemented in DynaFit, since increasing the stringency of the convergence criteria did not affect this result. The increase demonstrates that a slightly poorer fit is obtained as the quinonoid energy goes below ~ 4 kcal/mol, providing supporting evidence for the results presented in Figure 6.

that the true global minimum on the mean square hypersurface has been reached and for refining the values of the rate constants. This procedure was designed to eliminate any bias of the experimentalist and to ensure that the mean square hypersurface is broadly sampled for solutions.

Accuracy of the Free Energy Profiles. Five different types of evidence are presented here in support of the accuracy of

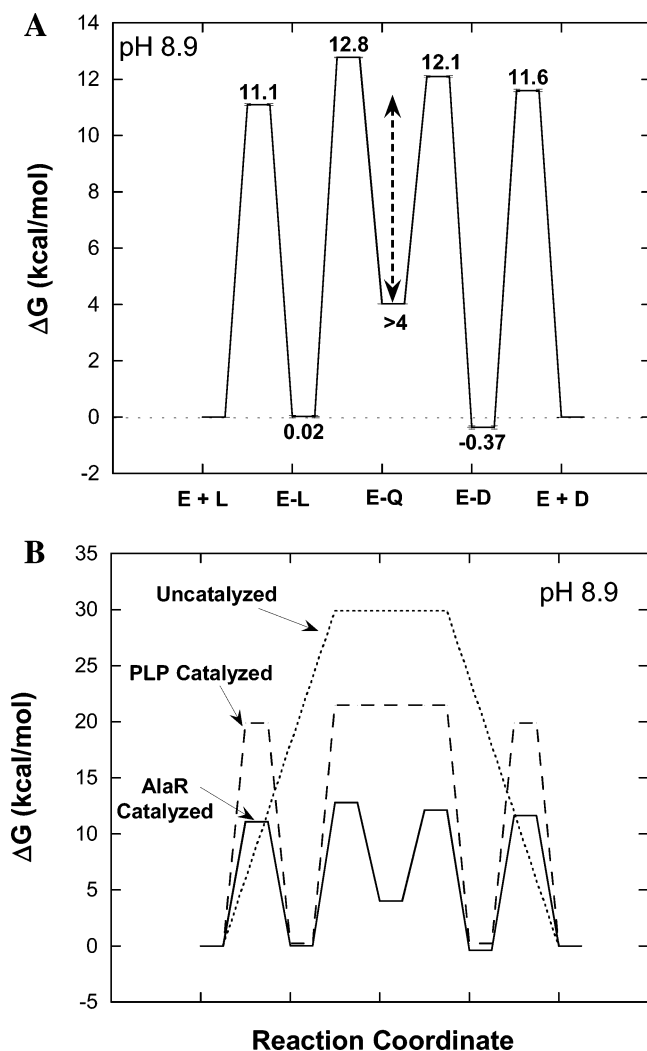


Figure 8. (A) Free energy profile for the pH 8.9 data set for a standard state of 5 mM, calculated from optimized rate constants in Table 2. The double arrow represents the region of uncertainty for the quinonoid intermediate, which extends to a lower limit of approximately 4 kcal/mol. (B) Overlay of free energy profiles for alanine racemase catalyzed, PLP catalyzed, and uncatalyzed alanine racemization at pH 8.9.

the free energy profiles. The first is the agreement between the experimental steady-state kinetic constants and those calculated from the free energy profiles. This criterion has the statistical disadvantage of not being completely independent of the fitting procedure, since it was used in the initial screening of the 1000 quasi-random rate constant sets and in the choice of rate constant sets that were averaged after the initial global fitting. Nonetheless, the free energy profiles could only be considered accurate if they were to reproduce the values of the experimental steady-state kinetic constants. In fact, they do this extraordinarily well as demonstrated in Table 1.

The second piece of experimental evidence in support of the accuracy of the free energy profiles is the viscosity dependence of alanine racemase at the high and low pH values. The pH 8.9 free energy profile presented in Figure 8A predicts the two proton transfers to C α to be both partially rate limiting. The two external aldimine formation reactions together are predicted to be 12% rate limiting for k_{cat}/K_M by a calculation of initial rates at low substrate concentration (0.1 mM) for the free energy profile and a hypothetical free energy profile in which the

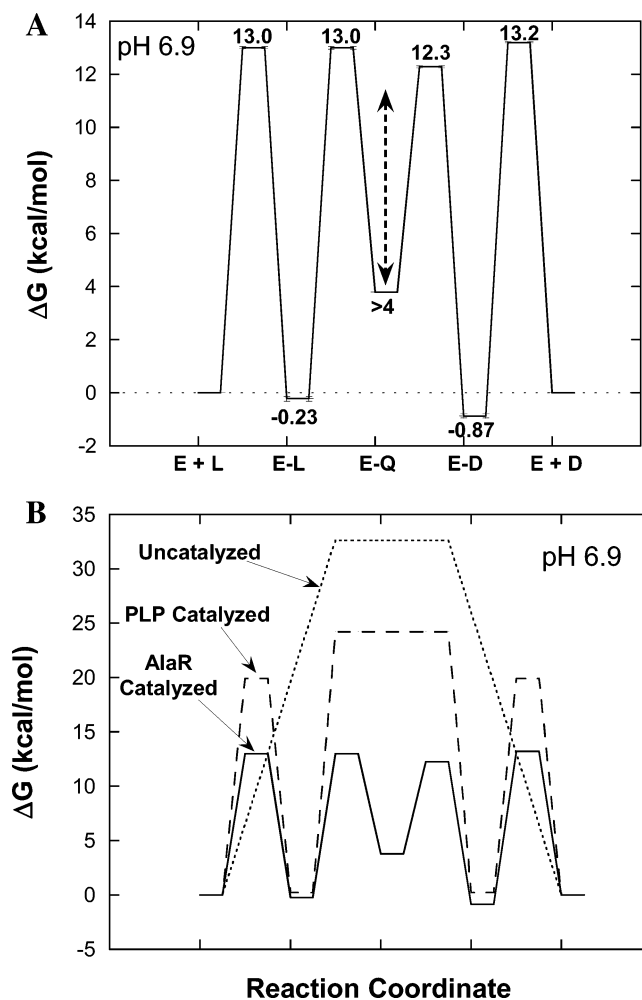


Figure 9. (A) Free energy profile for the pH 6.9 data set for a standard state of 5 mM, calculated from optimized rate constants in Table 3. The double arrow represents the region of uncertainty for the quinonoid intermediate, which extends to a lower limit of approximately 4 kcal/mol. (B) Overlay of free energy profiles for alanine racemase catalyzed, PLP catalyzed, and uncatalyzed alanine racemization at pH 6.9.

external aldimine formation steps had free energy barriers of only 5 kcal/mol (i.e., kinetically insignificant). A similar calculation for the pH 6.9 free energy profile predicts the external aldimine formation steps to be 66% rate limiting. The experimental data presented in Figure 1 show alanine racemase to be approximately 0% and 54% limited by viscosity dependent processes. This is in good qualitative agreement with the predictions from the free energy profiles, with the discrepancies likely arising from errors in the experimental measurements.

The third evidence in support of the free energy profiles concerns the energy of the quinonoid intermediate. The free energy profiles combined with the analyses presented in Figures 6 and 7 predict that the energy of the carbanionic quinonoid intermediate is at least 4 kcal/mol higher in energy compared to free enzyme and substrate. The absorbance spectra presented in Figure 2 confirm this prediction. There is a significant reduction in the 420 nm band attributable to the aldimine intermediates when saturating D,L-alanine is added, yet no significant positive difference peak is observed in the 480–550 nm range, where quinonoid intermediates are known to absorb.³⁸ The lower limit on the free energy calculated for the quinonoid intermediate from the spectral data is 4.2 kcal/mol

Table 4. Calculated Forward Commitment Factors and Intrinsic Kinetic Isotope Effects for pH 8.9^a

	observed KIE ^b	calculated c_f	calculated k^k
Substrate			
L→D ^c	1.877 (0.007)	0.061 (0.004)	1.93 (0.13)
D→L ^c	1.297 (0.012)	0.45 (0.05)	1.43 (0.20)
Solvent			
L→D ^d	1.06 (0.08)	3.64 (0.37)	1.33 (0.12)
D→L ^d	1.63 (0.09)	0.42 (0.03)	1.98 (0.15)

^a The errors on the observed KIEs are standard deviations from an average of three independent determinations. The errors on c_f are propagations of standard error estimates on individual rate constants obtained from DynaFit global analyses. The commitment factors are calculated from the optimized rate constant set in Table 2. The errors on the calculated KIEs are propagations of the errors reported for the observed KIE and the calculated c_f . ^b The observed kinetic isotope effect values are taken from previous work.⁷ ^c The commitment factors and intrinsic isotope effects are for abstraction of the C α proton from alanine in the L→D and D→L directions, respectively. ^d The commitment factors and intrinsic isotope effects are for donation of a solvent-derived proton to C α from the catalytic base in the L→D and D→L directions, respectively.

higher than that of the aldimine intermediates, in agreement with that predicted from the free energy profiles.

The fourth line of evidence consistent with the free energy profiles is provided by experiments in which racemization progress curves in D₂O are monitored. Cardinal and Abeles showed with proline racemase that the enzyme catalyzed progress curve in D₂O “overshoots” the stereoisomeric equilibrium (i.e., zero optical rotation) transiently, eventually returning to it.⁴⁴ This phenomenon occurs when there is insignificant exchange of C α protons of the substrate pool with solvent-derived protons. Of course, the product pool C α is fully deuterated at all times, since the proton transferred to C α is always solvent-derived. At the first point in the reaction, where there is an equal concentration of stereoisomers, there is an unequal distribution of hydrogen isotopes at C α in the substrate and product pools. That is to say, substrate has protium at C α , while product has deuterium at C α . This isotopic difference between the substrate and product pools causes different reaction rates for the forward and reverse reactions, determined in magnitude by the KIE, and thereby an overshoot of the stereoisomeric equilibrium. Another way of viewing this is that at the initial point of stereoisomeric equilibrium the system is not at isotopic equilibrium.

The data presented in Figure 3 show that the alanine racemase catalyzed reaction yields an overshoot of the stereoisomeric equilibrium in the L→D direction but not in the D→L direction at pH 8.9. Overshoot experiments were simulated with DynaFit using the pH 8.9 free energy profile presented in Figure 8A, the kinetic isotope effects in Table 4, and assuming rapid proton exchange between the quinonoid intermediate and solvent. The results of the simulation are in full agreement with the experimental results; an overshoot is observed only in the L→D direction. The different behavior in the forward and reverse directions is due to the difference in relative rates of C α –H washout for the stereoisomers.

The fifth supporting evidence is provided by the KIEs presented in Table 4. The substrate KIE in the L→D direction

reports on the vibrational differences between the C–H bond in the ground state and the bonding in the transition state. The solvent KIE in the opposite D→L direction reports on the same transition state but with the ground-state being the O–H bond on Tyr265. The equilibrium KIE for proton transfer between a hydroxyl group and the C α carbon of an amino acid is calculated to be ~ 1.13 .⁴⁵ Thus, one expects the intrinsic L→D substrate and D→L solvent KIEs to differ only by this factor. Calculation of the intrinsic KIEs from the observed values requires explicit values for commitment factors.⁴¹ Here, these commitment factors were calculated from the rate constants in Table 2, which determine the free energy profile. Thus, the accuracy of the calculated commitments provides a check on the accuracy of the free energy profile.

The last column of Table 4 presents the intrinsic KIEs calculated using the commitment factors derived from the rate constants in Table 2. There is remarkable agreement between the substrate KIE for one direction and the solvent KIE for the opposite. The L→D substrate and D→L solvent KIEs are identical within error, as are the D→L substrate and L→D solvent KIEs. The expected $\sim 13\%$ differences in these values are lost in the combined error of the KIE measurements and propagated errors from the commitment calculations, although the D→L substrate and L→D solvent KIEs do show the correct trend.

It seems prudent at this point to consider the theoretical limitations to the determination of free energy profiles using global analysis of progress curves. Intuitively, the main limitation is the inability to determine the value of a rate constant that never contributes significantly to rate limitation under any of the experimental conditions employed in the measurements. The free energy profile for pH 8.9 is used here to illustrate this point. Consider the 11.1 kcal/mol energy barrier for the formation of the L external aldimine intermediate at a standard state of 5 mM substrate (physiological concentration). At the highest initial concentration of substrate employed (20 mM), that barrier is decreased to 10.3 kcal/mol and does not contribute significantly to rate limitation. At the lowest concentration of substrate employed (0.2 mM), that same barrier has a value of 13.0 kcal/mol and is substantially rate limiting. Thus, one expects that the value of this rate constant is largely defined by the data collected at low substrate concentrations. If this rate constant was substantially larger (e.g., 100-fold), then the concentration range used here would not have contained sufficient information to define the value of this rate constant, since it would never have contributed significantly to rate limitation. This issue of rate limitation is the source of difficulty here in defining the values of k_4 and k_5 , the rate constants for quinonoid decomposition. These steps are very fast and do not contribute significantly to rate limitation under any of the experimental conditions used here.

Interpretation of the Free Energy Profiles. The individual free energy profiles presented in Figures 8A and 9A are compared to their nonenzymatic counterparts in Figures 8B and 9B. The free energy profiles for the C α deprotonation reaction of glycine with hydroxide is shown as the “uncatalyzed” reaction. The rate constant for this reaction was taken from the work of Richard et al.⁴⁰ The free energy profiles for the reaction of alanine and PLP to give Schiff base formation followed by deprotonation by hydroxide is denoted as “PLP catalyzed”. The

(44) Cardinale, G. J.; Abeles, R. H. *Biochemistry* **1968**, *7*, 3970–8.(45) Cleland, W. W. *Methods Enzymol.* **1980**, *64*, 104–25.

rate data for this profile were combined from two separate studies from Bruice's laboratory.^{3,39} No experimental information on the existence or energy of carbanionic intermediates in either the uncatalyzed or PLP catalyzed reactions was found in the literature. Therefore, this intermediate is not included in the nonenzymatic free energy profiles.

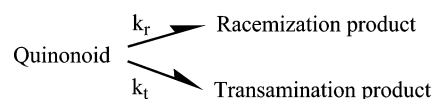
The addition of PLP to the deprotonation reaction at pH 8.9 lowers the free energy for deprotonation with respect to the reaction of alanine alone by 8.6 kcal/mol (a kinetic factor of 2.1×10^6). At pH 6.9 this value is 8.4 kcal/mol. This reduction in free energy is achieved through a change in mechanism, since the PLP catalyzed reactions occur via the aldimine intermediates. The addition of apo-alanine racemase to the PLP catalyzed reaction leads not only to further catalysis of the deprotonation step (free energy reduction of 8.7 kcal/mol at pH 8.9 and 11.0 kcal/mol at pH 6.9) but also to catalysis of aldimine formation by 8.8 kcal/mol at pH 8.9 and 7.0 kcal/mol at pH 6.9. The net reductions in the free energy of racemization are ~ 17 kcal/mol and ~ 19 kcal/mol at pH 8.9 and pH 6.9, respectively, corresponding to catalytic rate enhancements of $\sim 3 \times 10^{12}$ and $\sim 1 \times 10^{14}$, respectively.

Albery and Knowles considered three basic mechanisms for enzyme catalysis in their classic paper on triosephosphate isomerase.⁸ These are (1) uniform binding of all internal states, (2) differential binding of internal states, and (3) catalysis of elementary steps. At pH 8.9, the optimum for alanine racemase, the flux through the enzyme under second-order reaction conditions, could be slightly increased by additional increases in uniform binding of the internal states. For example, if the internal states at pH 8.9 were bound uniformly 0.5 kcal/mol more tightly, there would be only a $\sim 20\%$ reduction in the net rate constant, yet the enzyme would be 2.3-fold more saturated by substrate, representing a kinetic advantage of ~ 2 -fold at low substrate concentrations. Larger increases in uniform binding would rapidly become counterproductive. The situation at physiological pH (6.9) is different. Here, k_7 largely rate limits the forward L \rightarrow D reaction, while k_2 is already partially rate limiting for the reverse. In this case increasing uniform binding would not help the flux through the enzyme, and the enzyme is fully optimized in this regard.

The enzyme could benefit substantially at pH 8.9 from increased differential binding of the quinonoid intermediate. If one assumes that the proton transfer transition states are equidistant between the aldimine and quinonoid intermediates, then a lowering of the quinonoid intermediate energy by 4 kcal/mol would have the effect of lowering the proton transfer transition states by 2 kcal/mol, at which point they would no longer be significantly rate limiting. Again, the situation is different at pH 6.9. Here, only a small kinetic advantage would be incurred by lowering the quinonoid energy, since the proton transfer between the L external aldimine and the quinonoid is only partially rate limiting.

The third possibility, catalysis of elementary chemical steps in the mechanism is the means by which alanine racemase could most benefit catalytically. The enzyme could continue to evolve to the point that the second-order steps are equivalent to the rate constant for diffusional collision between the active site and the substrate ($6 \times 10^8 \text{ M}^{-1} \text{ s}^{-1}$ ⁴⁶). If the energies of the two proton transfer transition states were also lowered by the

Scheme 2



same factor (~ 4.3 kcal/mol at pH 6.9), then a net rate enhancement of ~ 1500 -fold would be achieved. Although alanine racemase is an impressive catalyst ($k_{\text{cat}} \sim 1000 \text{ s}^{-1}$ at pH 8.9 and $\sim 200 \text{ s}^{-1}$ at pH 6.9) for removing an unactivated proton from a C–H bond (amino acid $\text{C}\alpha\text{–H}$ $\text{p}K_{\text{a}} \sim 29$ ⁴⁰), it could still benefit substantially from evolutionary improvement implemented in the form of catalysis of elementary steps. The values of the enzyme efficiency functions defined by Albery and Knowles are 8.7×10^{-4} and 1.6×10^{-4} for pH 8.9 and 6.9, respectively. This can be compared to a value of 0.6 for triose phosphate isomerase.⁸

The most striking feature of the free energy profiles is the high energy of the quinonoid intermediate. Quinonoid intermediates are frequently observed as relatively stable species in PLP dependent enzyme reactions.³⁸ The high energy of the alanine racemase quinonoid intermediate is probably mostly determined by the Arg219 interaction with the pyridine nitrogen.⁴⁷ Many enzymes in which quinonoid intermediates are observed have instead a carboxylic acid group from aspartate or glutamate interacting with the pyridine nitrogen. The $\text{p}K_{\text{a}}$ of the guanidinium group of the arginine side chain (12.6) is much higher than that of a pyridinium ion (~ 5), prohibiting proton transfer, while carboxylic acid $\text{p}K_{\text{a}}$'s are matched to that of the pyridine nitrogen. In fact, the quinonoid intermediate was observed spectroscopically in the R219E mutant of alanine racemase, which has ~ 1000 -fold reduced activity.⁶

There must be a mechanistic imperative for this high energy quinonoid intermediate. It is proposed here to be the maintenance of high racemization specificity (i.e. prevention of side reactions). Alanine racemase has the highest known reaction specificity of all PLP enzymes. It undergoes transamination as a side reaction only 1 in 2×10^7 turnovers.⁴⁸ This corresponds to a 10 kcal/mol activation free energy difference between protonation of the quinonoid intermediate on $\text{C}\alpha$ (racemization) and $\text{C}4'$ of the coenzyme (transamination). One can rationalize the high quinonoid energy for the sake of reaction specificity using a simple parallel kinetics analysis. Making the reasonable assumption that the rate-limiting step for transamination is the movement of either Tyr265 or Lys39 into close proximity to $\text{C}4'$ of the coenzyme, the yield of racemization vs transamination products from the quinonoid intermediate will increase as the rate constant for proton transfer to the quinonoid intermediate is increased. Consider the simple parallel mechanism shown in Scheme 2. The fractional yield of racemization product is given by $k_r/(k_r + k_t)$. It is only increased by increasing the rate constant for proton transfer to the quinonoid (k_r) given the constancy of the rate constant (k_t) for the rate limiting conformational fluctuation required for transamination. That is to say, increasing the quinonoid energy increases reaction specificity by kinetically disfavoring the transamination side reaction.

A comparison of the free energy profiles for pH 8.9 and 6.9 shows that the proton transfer transition states are relatively

(47) Stamper, G. F.; Morollo, A. A.; Ringe, D. *Biochemistry* **1999**, *38*, 6714.
(48) Kurokawa, Y.; Watanabe, A.; Yoshimura, T.; Esaki, N.; Soda, K. *J. Biochem.* **1998**, *124*, 1163–1169.

(46) van Holde, K. E. *Biophys. Chem.* **2002**, *101–102*, 249–54.

unaltered by pH where the largest effects are on the external aldimine formation steps. These latter steps incur 1.9 and 1.6 kcal/mol increases in barrier heights as the pH is lowered from 8.9 to 6.9. The mechanism employed here (Scheme 1) is a minimal mechanism, and the first step (external aldimine formation) is in reality a complex process.⁷ External aldimine formation encompasses a minimally diffusive encounter between the substrate and the active site, followed by gain of access to the binding site, and subsequent Schiff base interchange with the internal aldimine (i.e., PLP-Lys39 aldimine). The increases in the barrier heights for external aldimine formation on going from pH 8.9 to pH 6.9 correspond to ~25- and ~15-fold decreases in rate constants for the L and D isomers, respectively. These decreases cannot be accounted for fully by changes in the protonation states of the enzyme or substrate; a factor of ~8-fold remains.⁶ Therefore, some of the changes in these composite barriers may come from the pH dependence of gating of substrate access to its binding site due to conformational fluctuations.^{49,50} The value of $k_{\text{cat}}/K_{\text{M}}$ for alanine racemase is relatively small ($\sim 1 \times 10^5 \text{ M}^{-1} \text{ s}^{-1}$) compared to theoretical limits for the diffusional encounter between substrates and enzyme active sites ($6 \times 10^8 \text{ M}^{-1} \text{ s}^{-1}$),⁴⁶ weighing against the collisional encounter being either rate limiting or the source of the dependence of $k_{\text{cat}}/K_{\text{M}}$ on viscosity at pH 6.9 (Figure 1). Rather, it appears most congruous that the conformational fluctuations required in the partially rate-limiting gating process at pH 6.9 are the source of the viscosity dependence. Gating has been proposed in the literature to be a source of substrate specificity.⁴⁹ There exist several examples in the literature where $k_{\text{cat}}/K_{\text{M}}$ values are much lower than the diffusion rate constant,

(49) Zhou, H. X.; Wlodek, S. T.; McCammon, J. A. *Proc. Natl. Acad. Sci. U.S.A.* **1998**, *95*, 9280–3.

(50) Scott, E. E.; Gibson, Q. H.; Olson, J. S. *J. Biol. Chem.* **2001**, *276*, 5177–88.

yet they still show viscosity dependence on this kinetic constant.^{28,51–56} This could generally be due to viscosity dependent conformational fluctuations being partially rate limiting.

The calculated intrinsic KIEs reported in Table 4 provide a measure of transition state structure. Theoretical limits on the values of primary deuterium KIEs are in the range 6–7.^{57,58} The magnitude decreases as the asymmetry of the transition state increases. The values of ~2 for the C–H/D–O transfer between substrate and Tyr265 and ~1.4 for the C–H/D–N transfer between substrate and Lys39 are indicative of a significant degree of asymmetry in bonding at the transition states. Unfortunately, without supplementary information one cannot say for certain whether the transition states are early or late. Given the high energy of the quinonid intermediate compared to the aldimines and the conceptual framework of the Hammond postulate, it is most probable that the transition states for proton removal from C α are late or, conversely, that the transition states for proton donations to the quinonoid are early.

Acknowledgment. This work was supported by U.S. National Institutes of Health Grant NIGMS 54779 to M.D.T..

Supporting Information Available: DynaFit script used in the processing of pH 8.9 and 6.9 data. This material is available free of charge via the Internet at <http://pubs.acs.org>.

JA049579H

(51) Hardy, L. W.; Kirsch, J. F. *Biochemistry* **1984**, *23*, 1275–82.

(52) Su, Q.; Klinman, J. P. *Biochemistry* **1999**, *38*, 8572–81.

(53) Mattei, P.; Kast, P.; Hilvert, D. *Eur. J. Biochem.* **1999**, *261*, 25–32.

(54) Li, Y.; Feng, L.; Kirsch, J. F. *Biochemistry* **1997**, *36*, 15477–88.

(55) Guha, M. K.; Vander Jagt, D. L.; Creighton, D. J. *Biochemistry* **1988**, *27*, 8818–22.

(56) Brouwer, A. C.; Kirsch, J. F. *Biochemistry* **1982**, *21*, 1302–7.

(57) Klinman, J. P. Primary Hydrogen Isotope Effects. In *Transition states of Biochemical Processes*; Gandour, R. D., Schowen, R. L., Eds.; Plenum Press: New York, 1978; pp 165–200.

(58) Westheimer, F. H. *Chem. Rev.* **1961**, *1*, 265.